dans le cas où l'un des cristaux a une épaisseur faible par rapport à l'autre. Il est possible également de calculer le contraste de franges de moiré obtenus avec deux cristaux d'épaisseur quelconque. La méthode de calcul dans ce cas serait la même que celle employée dans l'article précédent pour le calcul du contraste d'une faute d'empilement.

### Références


AUTHIER, A. (1966). *J. de Physique*, **27**, 57.

AUTHIER, A., LALLEMAND, P. & PFISTER, J. C. (1963). *J. de Physique*, **24**, 467.

AUTHIER, A. & MONTENAY-GARESTIER, M. T. (1965). *Effets des rayonnements sur les semi-conducteurs* (Paris-Royaumont, 1964), page 79. Paris: Dunod.

AUTHIER, A. & SIMON, D. (1968). *Acta Cryst.* A**24**, 517.

BASSET, G. A., MENTER, J. W. & PASHLEY, D. W. (1958). *Proc. Roy. Soc.* A**246**, 345.

BONSE, U. & HART, M. (1966). *Z. Physik*, **190**, 455.

BRÁDLER, J. & LANG, A. R. (1968). *Acta Cryst.* A**24**, 246.

CHIKAWA, J. I. (1965). *Applied Physics Letters*, **7**, 193.

GEVERS, R. (1962). *Phys. Stat. Sol.* **3**, 1672.

GEVERS, R. (1963). *Phys. Stat. Sol.* **3**, 2289.

HASHIMOTO, H., MANNAMI, M. & NAIKI, T. (1961). *Phil. Trans.* A**253**, 459.

LALLEMAND, P. (1962). Diplôme d'Études Supérieures, Paris.


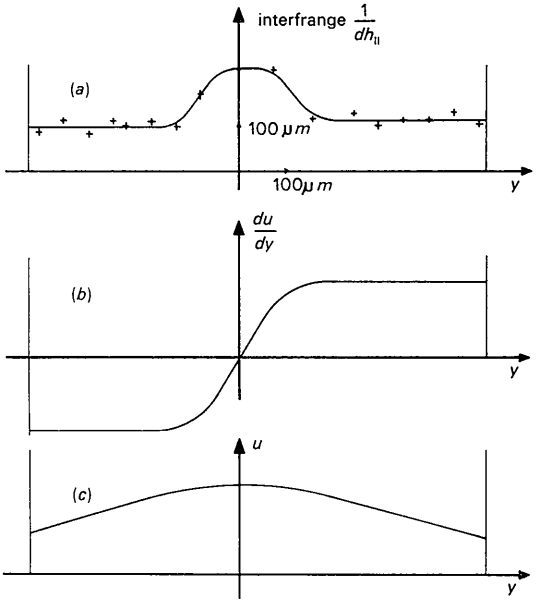


Fig. 8. Courbes représentant $1/dh$, $du/dy$ et $u$ en fonction de $y$.


LANG, A. R. & MIUSCOV, V. F. (1965). *Applied Physics Letters*, **7**, 214.

TAKAGI, S. (1962). *Acta Cryst.* **15**, 1311.


*Acta Cryst.* (1968). A**24**, 534

# The Analog Computation of Dynamic Electron Diffraction Intensities


BY A. W. S. JOHNSON

*Division of Chemical Physics, C.S.I.R.O., Chemical Research Laboratories, Melbourne, Australia*


(*Received* 18 *December* 1967)


The Cowley–Moodie slice formulation of $n$-beam electron diffraction has been manipulated to give a set of linear first order differential equations, one per beam, the coefficients of which are proportional to the Fourier coefficients of the crystal potential. The analog solution of these equations gives a vivid demonstration of the interacting processes involved in dynamic scattering and, with modern analog computers, allows an extremely rapid solution, at least two orders of magnitude faster than comparable digital computer calculations. The advantages and disadvantages of the method are discussed and practical example calculations and applications described.


## 1. Introduction

The use of analogies as an aid to the quantitative or qualitative interpretation of dynamic diffraction theory was clearly envisaged by Ewald, when he described the 'Pendellösung' solution, and was freely invoked by Brillouin (1946). In addition, Heidenreich (1950) constructed a useful analogy by utilizing the correspondence between the dispersion equations and those of a suitable electrical network. However, since the dispersion equations are the result of formal mathematics invoked solely for the purpose of calculation and are not essential to the solution of the diffraction problem, the analogy is of limited value and only indirectly connected with experimentally observed quantities.

The direct solution of the differential equation formulation of the diffraction theory (Tournarie, 1961; Takagi, 1962) has the advantage, in common with the multislice calculation of Goodman & Moodie (1968), of avoiding the unnecessary solution of the dispersion equations, the wave functions external to the crystal being calculated directly. Consequently the electrical network resulting from programming an electronic analog computer to solve these differential equations

offers an immediate and a powerful analogy to the process of dynamic electron diffraction.

In this paper the advantages, limitations and uses of analog methods will be discussed with reference to particular calculations, and some results compared with equivalent digital calculations. Practical details for implementing the technique are described. A derivation of the differential equation form of the theory from the slice formulation of Cowley & Moodie is given as it demonstrates the theoretical connexion between the digital multislice and analog methods of calculation.

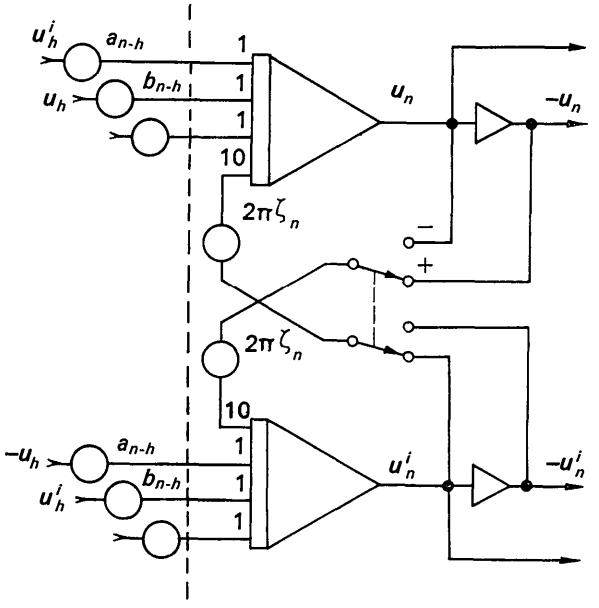


Fig. 1. A beam unit. The basic assemblage of computing components required per beam is shown on the right of the dotted line in standard analog computer programming symbols (Korn & Korn, 1964, p. 6). The inputs from other beams enter from the left and voltages representing the real and imaginary parts of the $n$th beam amplitude are available on the right.

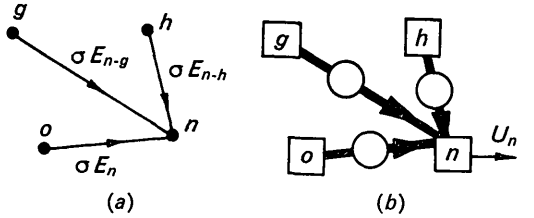


Fig. 2. Correspondence between the diffraction pattern and computer connexions. (*a*) The single scattering processes contributing to a beam $n$ are represented by vectors in the diffraction pattern. (*b*) A symbolic representation of the corresponding connexions between beam units. The broad arrows symbolize two wires in centrosymmetric and four in non-centrosymmetric cases. The potentiometers are similarly symbolic.

## 2. Theory

A formal derivation of a differential equation formulation of the $n$-beam diffraction problem can be made by starting from the Cowley–Moodie recurrence relation (Cowley & Moodie, 1957). This relation describes the wave function $\psi_m(x)$ at the exit face of a thin arbitrary slice of crystal† in terms of the wave function at the exit face of the previous slice $\psi_{m-1}(x)$, a propagation function $p(x)$ describing the phase changes due to propagation and a function $q_m(x)$ representing the phase changes resulting from the potential of the $m$th slice projected on to a two-dimensional sheet at the centre of the slice. Thus

$$\psi_m(x)=[\psi_{m-1}(x) * p(x)] \,.\, q_m(x) \,. \qquad (1)$$

It has been proved by A. F. Moodie (private communication) that the separation of phase changes due to propagation from those due to interaction implied by (1) gives an exact result with an appropriate limiting process when the crystal is divided into an infinite number of planes at infinitely small separation.

It is convenient to work from the Fourier transform of (1), written neglecting constant terms as

$$U_m(\theta) = [U_{m-1}(\theta) \,.\, \exp(-2ik\Delta z\theta^2)] * \mathscr{F}\{q_m(x)\} \,, \qquad (2)$$

where $U_m(\theta)$ is the transform of $\psi_m(x)$, the exponential term is the transform of the propagation function for the case of normal incidence,‡ $\Delta z$ is the distance between slice centres, $2\theta$ the angle between the incident wave and the direction of observation and $k$ the magnitude of the incident wave vector within the crystal corrected for relativistic effects. This is the equation evaluated repetitively in the digital multislice method of Goodman & Moodie.

For perfect crystal diffraction at discrete angles $\theta_n$, the last term in (2) can be written as

$$\mathscr{F}\{q_m(x)\}=\delta(\theta)+i\sigma\Delta z E_m(\theta) \sum_n \delta(\theta-\theta_n)$$

$$-\frac{\sigma^2\Delta z^2}{2!}[E_m(\theta) \sum_n \delta(\theta-\theta_n) * E_m(\theta) \sum_n \delta(\theta-\theta_n)]+\ldots$$

since $q_m(x)=\exp\{i\sigma\Delta z\varphi(x,z_m)\}$ (Cowley & Moodie, 1957). Here $\sum_n \delta(\theta-\theta_n)$ represents an infinite set of delta functions, $\sigma=\frac{k}{2W}\frac{2}{\{1+(1-\beta^2)^{1/2}\}}$,§ where $W$ is the

† For convenience only two dimensions will be considered, $x$ being the lateral coordinate and $z$ the coordinate perpendicular to the slice. The extension of the results to three dimensions is straightforward.

‡ In electron diffraction it is sufficient to make a small angle approximation when constructing $p(x)$. We have used $p(x)=\frac{1}{\Delta z}\exp(ikx^2/2\Delta z)$.

§ The factor $2/\{1+(1-\beta^2)^{1/2}\}$ is the relativistic correction for mass; see Fujiwara (1961), Goodman & Lehmpfuhl (1967).

accelerating voltage and $E_m(\theta)$ is the Fourier transform of $\varphi(x,z_m)$, the one-dimensional distribution of potential in a slice centred at $z_m$, given by

$$E_m(\theta) = \int_{-\infty}^{\infty} \varphi(x,z_m) \exp(2ik\theta x) \,.\, dx \,.$$

If the incident wave can be represented as a delta function and $q_m(x)$ is periodic, the recurrence relation (2) shows that the functions $U_m(\theta)$ and $U_{m-1}(\theta)$ will have non-zero values only in the discrete directions $\theta_n$ and thus can be represented by column vectors with components $U_m(\theta_n)$. A typical element of (2) is then

$$U_m(\theta_n) = [U_{m-1}(\theta_n) \,.\, \exp(-2ik\Delta z\theta^2)] * [\delta(\theta_n) + i\sigma\Delta z E_m(\theta_n) + \ldots]$$

where $E_m(\theta_n) = \sum_l E(\theta_n, l) \exp(2\pi i z_m l/c)$, $E(\theta_n, l)$ being the Fourier coefficients of the crystal potential.

Taking sufficient terms to allow evaluation of the convolution correct to the first order in $\Delta z$ gives

$$\begin{aligned} U_m(\theta_n) &= \sum_h U_{m-1}(\theta_h)\{1 - 2ik\Delta z\theta_h^2\} \\ &\quad \times \{\delta(\theta_n - \theta_h) + i\sigma\Delta z E_m(\theta_n - \theta_h)\} \\ &= U_{m-1}(\theta_n) - 2ik\Delta z\theta_h^2 U_{m-1}(\theta_n) \\ &\quad + i\sigma\Delta z \sum_h E_m(\theta_n - \theta_h) \,.\, U_{m-1}(\theta_h) + \ldots \end{aligned} \tag{3}$$

By Taylor's theorem

$$U_m(\theta_n) = U_{m-1}(\theta_n) + \Delta z \frac{dU_{m-1}(\theta_n)}{dz} + \ldots . \tag{4}$$

Equating coefficients of $\Delta z$ between (3) and (4) results in the limit of $\Delta z \to 0$ in a set of $n$ simultaneous differential equations

$$\begin{aligned} \frac{dU(\theta_n)}{dz} &= -2ik\theta_n^2 U(\theta_n) \\ &\quad + i\sigma \sum_h E_m(\theta_n - \theta_h) \,.\, U(\theta_h) \,. \end{aligned} \tag{5}$$

Extension of the arguments to the three-dimensional case leads to the same equations, the indices $n$ and $h$ being taken to include all desired reflexions in the zero layer. The effects of upper layer reflexions enter through the term $E_m$.

The equations used for analog computation were generalized to include cases other than normal incidence by replacing $2k\theta_n^2$ by $-2\pi\zeta_n$ where $\zeta_n$ is the excitation error for an Ewald sphere of radius $1/\lambda$. With this modification and a simplified notation equation (5) becomes

$$\left.\begin{aligned} \frac{dU_o}{dz} &= 0 + i\sigma \sum_h E_{o-h} U_h \\ &\vdots \quad\quad \vdots \quad\quad \vdots \\ \frac{dU_n}{dz} &= i2\pi\zeta_n U_n + i\sigma \sum_h E_{n-h} U_h \end{aligned}\right\} . \tag{6}$$

Apart from a small angular approximation this equation is identical with that given by Tournarie (1961) for the case of negligible backscattering and is contained in more general differential equations due to Takagi (1962) and Howie & Whelan (1961) which include to a greater or lesser extent the influences of distortions within the crystal.

### 3. Analog computation

The programming of an electronic analog computer to solve the differential equations just described results in a computational network whose analytical properties

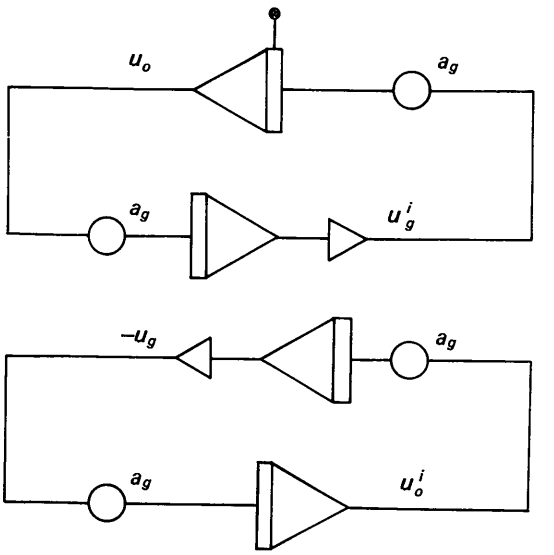


Fig. 3. Two-beam centrosymmetric case. Excitation error zero. An initial condition is shown on the upper integrator only, representing the incident beam with phase angle zero.

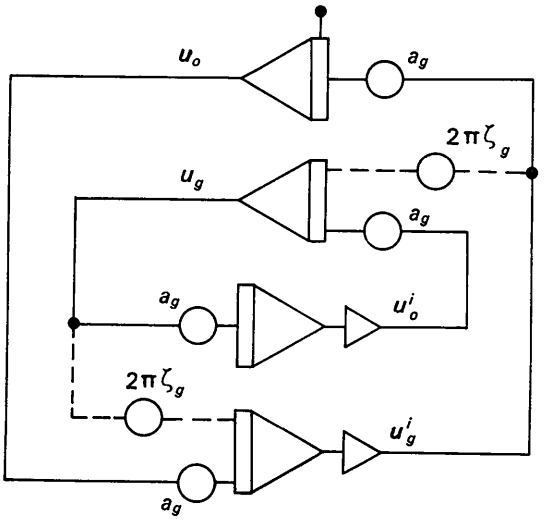


Fig. 4. Two-beam, excitation error connexions shown with dotted lines.

will be discussed in §4. For the present attention will be focused on constructing the network in a form which has been found suitable for making successful numerical computations with up to seven beams.

*Programming*

The representation of complex variables on conventional analog computers is best made with their real and imaginary components. It is then necessary to make the substitutions $U_n=u_n+iu_n^i$ and $\sigma E_n=a_n+ib_n$ in (6) and split each equation into real and imaginary parts before computation is possible. This results in pairs of equations of the following form

$$\left.\begin{aligned}\frac{du_n}{dz} &= -2\pi\zeta_n u_n^i - \sum_h (a_{n-h}u_h^i + b_{n-h}u_h)\\ \frac{du_n^i}{dz} &= 2\pi\zeta_n u_n + \sum_h (a_{n-h}u_h - b_{n-h}u_h^i)\end{aligned}\right\}, \quad (7)$$

it being noted that the effect of upper layer interactions has been omitted. Taking the independent computer variable time to represent $z$, the basic circuit for solving (7) is shown in Fig. 1,† one such circuit being required for each beam taken into consideration. It is convenient to refer to the portion of the circuit on the right of the dotted line as a beam unit as it includes all the components required per beam apart from those necessary for calculating intensity. The upper and lower integrators in Fig. 1 compute the real and imaginary components of the diffracted wave amplitude respectively and are followed by two inverters generating their negatives. The double pole switch, which facilitates the selection of the sign of the excitation error and the associated potentiometers are redundant in the case of the unit representing the central beam. The potentiometers to the left of the integrators are used to multiply the incoming amplitudes from other beams, $h$, by the real and imaginary components of the scattering probabilities $a_{n-h}$ and $b_{n-h}$. The interconnexions between the beam units *via* these potentiometers are readily deduced with the aid of two simple rules:

1. An integrator computing the real component can only have inputs which are imaginary, (*viz.* $u_h b_{n-h}$ or $u_h^i a_{n-h}$) and *vice versa.*

2. The coefficient potentiometer multiplying an incoming amplitude $u_h$ must be set to a value corresponding to the probability that electrons in the beam $u_h$ will be directly scattered into the direction of the beam $n$ being considered.

This probability is $\sigma E_{n-h}$ per unit length in the direction of the beam. The combinations of $u_h$ and $E_{n-h}$ required are conveniently determined from a map of reciprocal space showing all reflexions included in the calculation, as the connexions between the beam units of the analog computer have the same topology as the vectors between the reciprocal lattice points which represent the scattering of electrons from one beam to another. This is illustrated in Fig. 2. All connexions involving $a_0$ may be omitted, the diffraction pattern being independent of the real part of the zero order Fourier coefficient of the potential $E_0$.

As a result of the foregoing it is possible to program the analog computer directly from a diffraction pattern without reference to the differential equations.

† The effect of sign reversal which occurs with conventional electronic integrators has been allowed for in labelling all circuit diagrams in this paper.

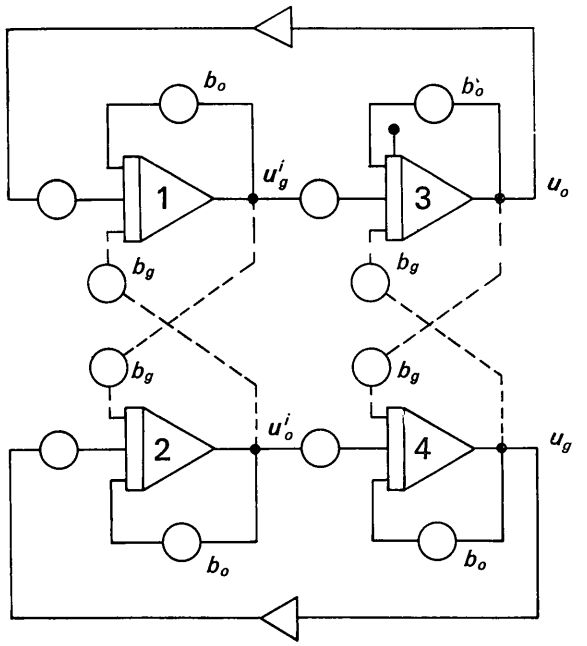


Fig. 5. The two-beam case with absorption. No excitation error. The potentiometers for $b_o$ simulate the angular independent absorption coefficient as they are equivalent to leaking integrating capacitors.

*Scaling*

Amplitude scaling is straightforward since the scattering process is interpreted in terms of probabilities. Since $\sigma_{80\text{kev}}\simeq 0{\cdot}001$ and for $E=10$ volts the coefficients $a$ are of the order of 0·01, a scale factor of $s=100$ Å.sec$^{-1}$ is often convenient, as it results in the Fourier coefficient potentiometers being set to $s\sigma E=1$. The computer then runs so that a second of real time corresponds to 100 Å of crystal thickness. With $s$ as 100 a sensible scaling of the excitation error potentiometers for typical values of $2\pi\zeta$ will result if they are connected to $\times 10$ inputs. For high-speed computation $s$ can be as great as $10^6$ Å.sec$^{-1}$.

*Initial conditions*

Integrator initial conditions corresponding to a plane wave incident on the crystal are simply $u_o=1$, $u_n=0$, $n\neq 0$ and $u_n^i=0$. Otherwise the calculation may be commenced from a point within the crystal by using a predetermined set of self consistent amplitudes as integrator initial conditions.

### 4. Properties of the analog network

In the previous section the programming of an analog computer for practical calculation was treated and a limited use made of the analogy between the diffraction pattern and the network of computing components. The analogous properties of the network may be employed more widely to explore the effects of excitation error, phases and symmetry in cases of three or more beams. The facility with which the network can be used for such purposes is readily understood when it is recognized that it is in fact a diagrammatic picture of an operator representing the diffraction process. This operator acts on the incoming wave (analog computer initial conditions) to produce the diffraction pattern and so contains all the influences of wavelength, crystal and angle necessary to the problem.

The use of the analog network as a conceptual aid in dynamic diffraction is best illustrated by the following descriptions of excitation error, phase and absorption effects in two- and three-beam cases.

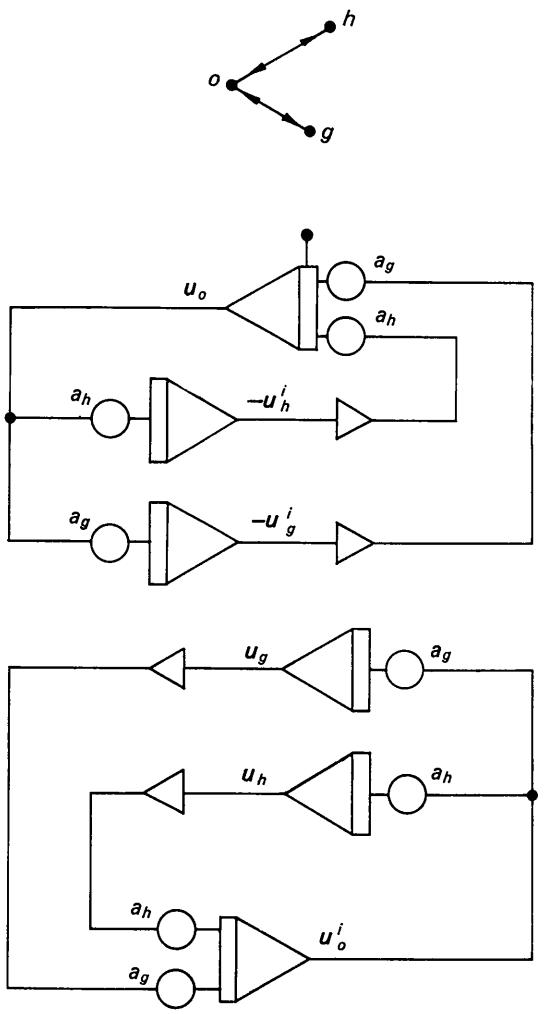


Fig. 6. Three-beam case. No excitation errors. The allowed coupling terms are shown in the upper diagram and the corresponding analog circuit below.

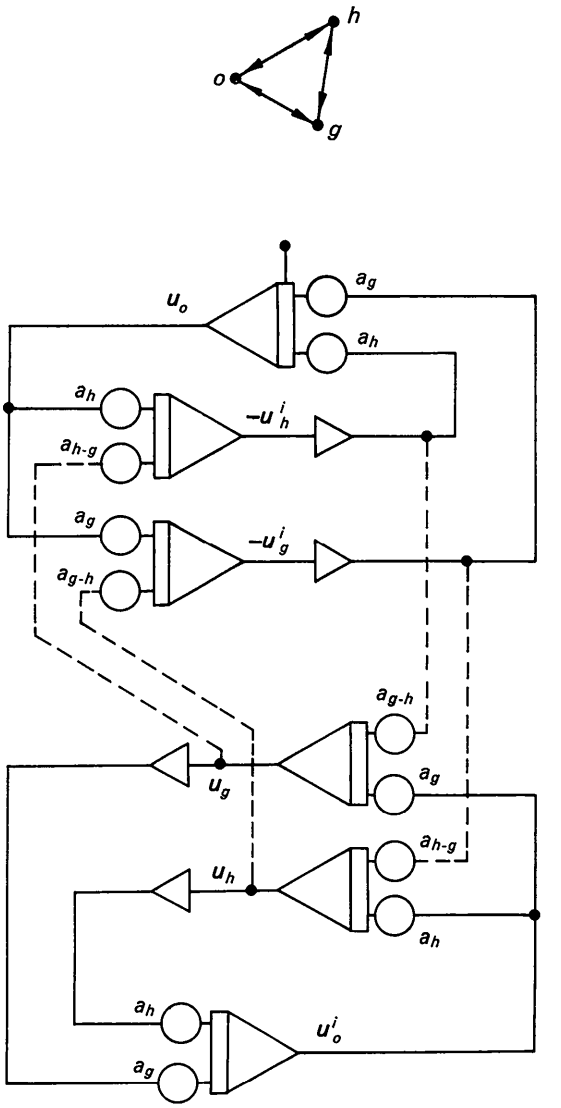


Fig. 7. Three-beam case as shown in Fig. 6 except that the $g-h$ coupling term is allowed, the dotted line connexions being introduced as a result.

*Two-beam case*

The beam unit arrangement of programming symbols has been found convenient for making practical calculations on an analog computer. However, for the present purposes another arrangement, taking advantage of the symmetry of the operator, is more readily comprehended. The two beam centrosymmetric case with no absorption or excitation error is shown in this latter arrangement in Fig. 3, the circuit being constructed using the rules set out in § 3. It will be observed that the two circuits which comprise this Figure both represent the equation of a simple pendulum written

in the simultaneous equation form

$$\frac{du_o}{dt} = -a_g u_g^i \; ; \qquad \frac{du_g^i}{dt} = a_g u_o \; .$$

If the phase of the incident wave is taken to be zero, oscillations will occur only in the upper circuit, the initial conditions in the lower circuit being zero. The addition of an excitation error introduces connexions between the upper and lower loops which increases the gain around the upper loop, and hence the frequency of oscillation, as shown in Fig. 4.

One would expect that the introduction of leaking integrator capacitors would produce an absorption like effect. Reference to equation (7) confirms that a calculation including a constant absorbing potential

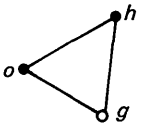


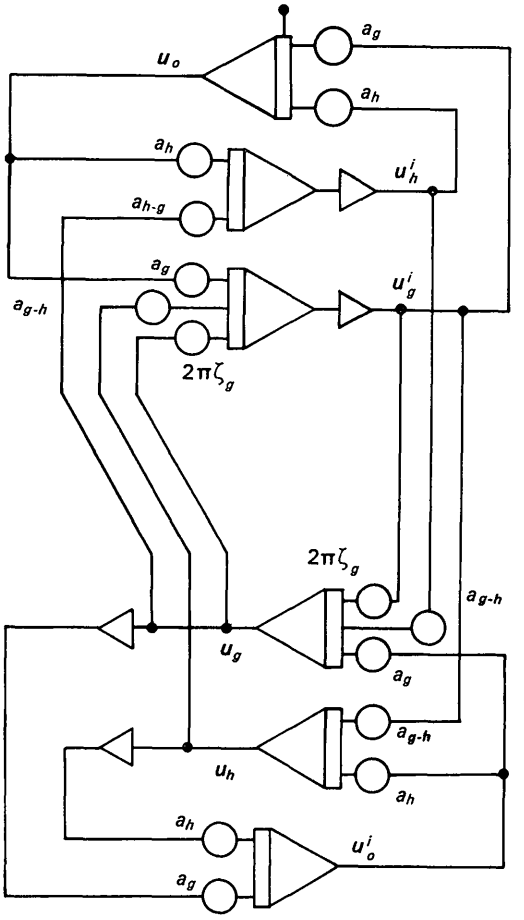


Fig. 8. Three-beam case with one positive excitation error, all coefficients positive. The open circle in the coupling diagram represents a non-zero excitation error.

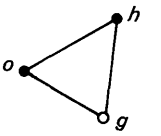


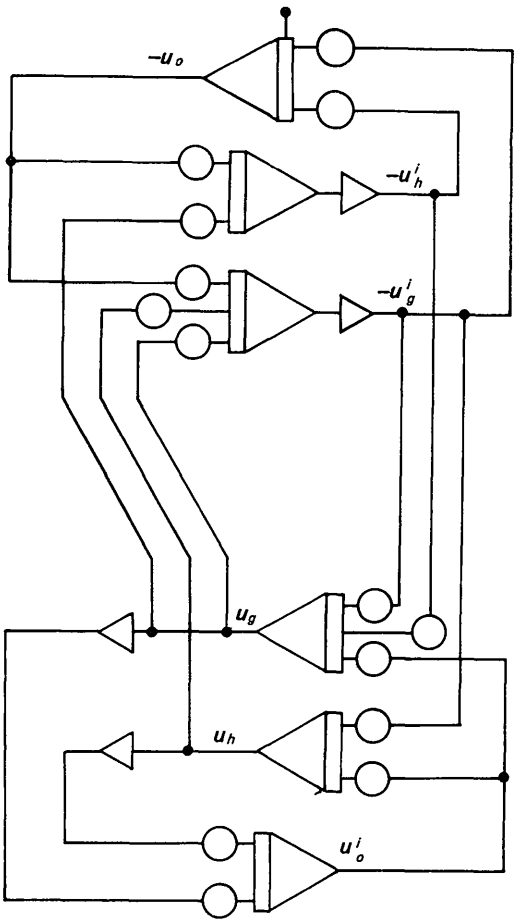


Fig. 9. Three-beam case, excitation error and $a_h$ now negative. The connexions are identical with those in Fig. 8.

($b_o > 0$, $b_g = 0$) requires resistors in parallel with all integrating capacitors as shown in Fig. 5, and that the absorption acts equally on all beams in the crystal in damping the solution. Structure in the absorbing potential ($b_g \neq 0$) is simulated by the dotted connexions between the upper and lower computational loops in Fig. 5, exciting oscillations in the lower loop. These connexions yield strong positive feedback between the integrators 1 and 2 and between 3 and 4. However this is directly offset by the negative feedback due to the zero order coefficient of the absorbing potential. A balance between these opposing connexions is maintained provided $b_o > b_g$, that is, so long as the absorbing potential remains positive. For $b_o < b_g$ the solution

diverges, corresponding to electrons being created in the crystal.

For $b_o = b_g$ a damped oscillation occurs, the intensity of both beams tending to a constant value of 0·25 for large $z$, the theoretically maximum possible Borrmann effect for zero excitation error.

*Three-beam case*

The diagram representing the two-beam theory in Fig. 3 can be extended to give some insight into the effects of a third beam, and by exploiting the symmetry of the diagrams the equivalence of say, excitation error and Fourier coefficient may be demonstrated in certain instances.

Initially, consider the case where the Bragg condition for two strong beams $g$ and $h$ is satisfied and no coupling term, $g-h$, exists. The coupling terms for the strong beams are both of positive sign. The corresponding analog circuit may be immediately drawn utilizing the rules given earlier and is shown in Fig. 6. From this circuit, it is clear that the solution will be of sinusoidal form, since all the components for the additional beam, $g$, are in parallel with those for the other beam, $h$, and both the integrators for these beams have the same initial conditions. The paralleling of components in the oscillating loops results in increased loop gain and a shortened extinction length. Inspection of the circuit shows this to be true even if the signs of the two coupling terms differ.

If the coupling term $g-h$ is now no longer zero, connexions between the upper and lower circuits of Fig. 6 are introduced as shown by the dotted lines in Fig. 7 for $a_{g-h}$ positive. By tracing out the additional loops it is found that similar components are paralleled, independent of the signs of the coupling terms, and consequently the extinction length will again be shortened.

If the sign of the coupling term $a_{g-h}$ becomes negative the dotted line connexions in Fig. 7 are each switched to the opposite sides of the inverters at their input ends. The resulting diagram is simply that of Fig. 7 turned up side down. Thus, since the upper and lower portions of the diagram are identical and the initial conditions may be applied to either the $u_o$ or $u_o^i$ integrators, the computed intensities are independent of the sign of $a_{g-h}$. Similar arguments may be used to show that the signs of the $g$ and $h$ terms are likewise unimportant and consequently no phase information is available when both excitation errors are zero. This result could be obtained in principle from the analytic expression for the dynamic theory of Cowley & Moodie (1962).

The introduction of an excitation error allows conclusions to be drawn concerning the phase of the three coupling terms as demonstrated by Kambe and Miyake (Kambe, 1954, 1957). This result may be obtained by an inspection of the circuit diagrams for various combinations of the signs of the three coupling terms and the excitation error. As an example, consider the circuit shown in Fig. 8 for the case where all four signs are positive. If, upon changing one or more signs the circuit remains unchanged or cannot be transformed by a simple inversion or relabelling back to the original, the diffracted intensities will also remain unchanged and no phase information can be obtained. For example changing the sign of the excitation error and $a_h$ simultaneously is equivalent to relabelling the circuit as shown in Fig. 9. Consequently the diffracted

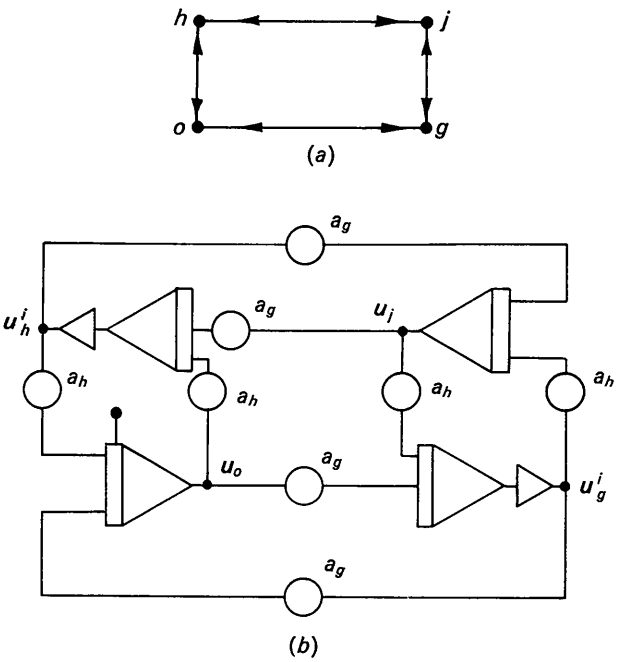


Fig. 10. (*a*) The scattering paths between two sharp beams *o* and *g* and their plasmon-excited beams *h* and *j*. (*b*) The corresponding computing circuit for all excitation errors zero.

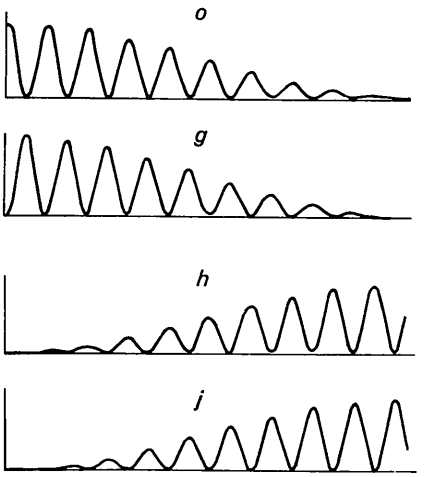


Fig. 11. Intensity *versus* thickness curves for the four beams computed by the circuit of Fig. 10(*b*) with $E_g = 2$ volts, $E_h = 0{\cdot}1$ volt. The transfer of energy from the sharp to the diffuse beams is clearly apparent.

intensities will remain unchanged. Likewise, changing the sign of $\zeta_g$ and $a_{h-g}$ simultaneously is equivalent to turning the circuit of Fig. 8 up side down and again no change results. Similar arguments to these show no change occurs when any two signs are simultaneously reversed. However, changing any one sign gives a new topology to the circuit which results in a different intensity being obtained. This new topology is maintained if subsequently two signs are changed simultaneously. The calculated intensity therefore depends upon the sign of the product $a_g \,.\, a_h \,.\, a_{h-g} \,.\, \zeta_g$ and since the sign of $\zeta_g$ can be measured experimentally the relative signs of the three Fourier coefficients may be obtained provided a sufficient number of comparisons are possible.

*Plasmon diffuse scattering*

The possibility of making qualitative calculations with a limited number of components is best illustrated by the following example in which the effect of diffuse scattering due to plasmon excitation in a two-beam situation was examined. This has been treated, for example, by Howie (1963). In all, four beams with zero excitation error were included, two sharp, $o$ and $g$ and two diffuse, $h$ and $j$, the permissible scattering paths between them being shown in Fig. 10(*a*). The rapid fall off of the plasmon scattering curve allows the sharp to diffuse processes $o-j$ and $h-g$, and their inverses, to be omitted. Because the terms $g-h$, $j-o$, their inverses and all the $\zeta$'s were zero and an even number of non-zero coupling terms were required, the computer circuit separated into two symmetric parts similar to those described earlier. Taking the phase of the central beam at the entrance face to be zero meant only that part of the circuit containing the integrator for $u_0$ was required, and this is shown in Fig. 10(*b*). The lower loop in the circuit representing the sharp beams initially contains all the energy which oscillates in a standard two beam fashion. However the upper loop representing two diffuse beams gradually extracts this energy *via* the sharp-diffuse connexions $o-h$ and $g-j$, resulting in the curves in Fig. 11. It will be appreciated that complete coherence between the sharp and diffuse waves is implied and consequently the calculation will be in error at large thickness.

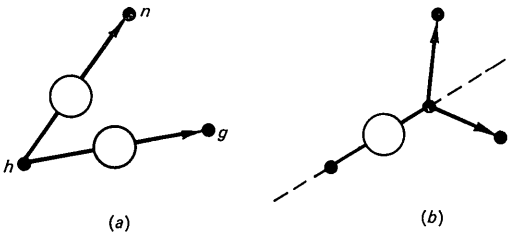


Fig. 12. An illustration of the effect of a mirror plane on the number of coefficient potentiometers required. If the coefficients $n-h$ and $g-h$ are equal and of the same sign, a mirror plane (dotted line) exists and circuit (*b*) can replace the general circuit (*a*).

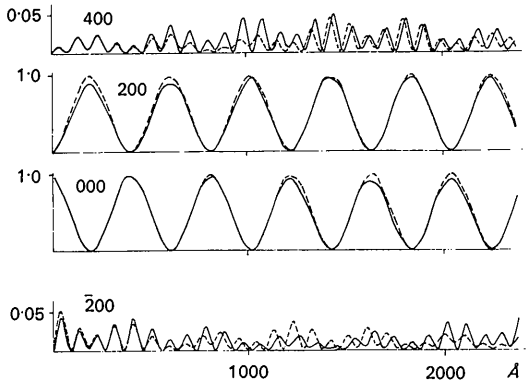


Fig. 13. Comparison of a one-dimensional four-beam analog computation (full lines) with a 14-beam digital computation (dotted lines). Conditions: $E_{200}=7{\cdot}065$ volts, $E_{400}=2{\cdot}939$ volts, $E_{600}=1{\cdot}751$ volts, $\zeta_{200}=0$, $\zeta_{400}=\zeta_{\bar{2}00}=-0{\cdot}00928$ Å$^{-1}$, $\sigma=0{\cdot}9936\times10^{-3}$ V$^{-1}$ Å$^{-1}$, $\lambda=0{\cdot}04092$ Å, $W=83{\cdot}13$ kV. Potential for digital computation calculated with 13 Fourier coefficients (HF scattering curves) and $B_{Mg}=B_O=0{\cdot}26$Å$^2$.

*The $\zeta$ pendulum*

The connexions introduced by a finite excitation error immediately suggest the manner in which this parameter affects the intensity of a beam. In Fig. 1 the connexions for $\zeta$ place two integrators and one of the two inverters in a closed loop which represents a pendulum of resonant frequency $s\zeta$ cps. The incoming waves act as forcing functions to this pendulum which will respond only slightly when $s\zeta$ is large compared with the frequency of the thickness fringes. Alternatively, small values of $\zeta$ will act mainly in shifting the phase of the incoming waves and have little effect on their amplitude.

## 5. Limitations and applications

In electron diffraction calculations a striking property of the analog computer is its speed relative to that of a digital machine. For example a four beam computation which took 2 minutes by digital methods was completed in 25 ms (scale factor $s=10^5$ Å.sec$^{-1}$) using a high speed analog computer with a computing bandwidth of $>50$ kc. This advantage is offset by the limited capacity of the analog computer; the maximum size of the calculation will be determined by the number of coefficient potentiometers available and the facility with which they can be set. Generally commercial computers have a more than adequate supply of integrators and inverters. For $n$ beams the maximum number of potentiometers required assuming all possible interactions and excitation errors are included is $2n^2-2$ for a centrosymmetric crystal with no absorption and $4n^2-2n-2$ for a non-centrosymmetric crystal or when absorption is included. In practice these numbers can be reduced, as often symmetry relations cause the same product $u_h a_{n-h}$ to occur more than

once in equations (7). This is illustrated in Fig. 12 for the case of a mirror plane.

Present experience suggests calculations with 8 to 10 beams to be the maximum practical size on general purpose, 100 amplifier machines.

*Accuracy*

Apart from errors due to the omission of beams, machine phase and amplitude errors influence the accuracy of analog computations. A qualitative measure of the latter errors is possible since the circuit can be dissected into loops representing simple harmonic oscillators and the errors in such loops have been well analysed (*e.g.* Korn & Korn, 1964, p. 114). However, the complexity of loops in the complete circuit makes a theoretical estimate of the errors intractable.

A simple method of estimating machine errors is to compare computed results with digital calculations,† a technique which will also allow errors due to the omission of weak beams to be investigated. The results of such a comparison are contained in Figs. 13, 14 and 15. The example in this case is a four-beam analog computation for MgO $h00$ systematics with the 200 reflexion exactly satisfied. Various digitally computed curves are shown, the first of which was obtained by including all the Fourier coefficients necessary for a reasonable representation of the one-dimensional potential (13 orders). The corresponding multi-slice calculation included all possible single scattering interactions between 14 beams, 4 of which are shown in Fig. 13 superimposed on the analog curves. Agreement in the $\bar{2}00$ and 400 reflexions was noticeably improved in a second digital calculation when the scattering potential was calculated using only those Fourier coefficients that were present in the analog computation. The subsequent phase grating and multi-slice calculations were completed using 14 beams and the results are shown in Fig. 14.

The two digital calculations just described both accurately portray diffraction from the respective potential models used, since sufficient numbers of beams were included to restrict the weak beam absorption to less than 0·1% and the convolution test of the thin phase grating amplitudes $F_h$, given by

$$\sum_{h'} F^*_{h'} \cdot F_{h+h'} = \begin{cases} 1 \text{ for } h=0 \\ 0 \text{ for } h\neq 0 \end{cases}$$

(Moodie, 1965; Goodman & Moodie, 1968), was correct to 1 in $10^6$. This is no longer true if the multi-slice calculation is restricted to the 4 beams computed by analog means, the weak beam absorption amounting to 20% after 2000 Å. However, after allowing for this absorption the agreement with the analog curves becomes excellent as shown in Fig. 15. It thus appears that within the limits of the example used, the accuracy of an analog computation is limited mainly by the omission of weak beams and not by machine errors.

*Further applications*

Some applications of the technique have already been described in §4. The programming ease, speed and versatility of modern analog computers will allow others to be readily envisaged and rapidly completed. One important modification to the circuit of Fig. 1 widens the scope of the method to include convergent beam patterns and $n$-beam diffraction from distorted crystals. The modification consists in connecting multipliers in parallel with the $\zeta$ potentiometers to allow changes in crystal orientation to be introduced rapidly during calculation.

For convergent beam patterns the computer is run repetitively for fixed periods of time (constant thickness) whilst introducing changes in $\zeta$ *via* the multipliers during the resetting interval between the computing periods. The gross tilt of the crystal is defined

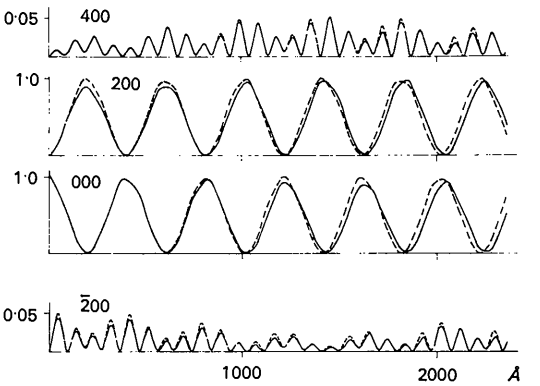


Fig. 14. Same as Fig. 13 except potential for digital computation constructed using only the 200, 400 and 600 Fourier coefficients.

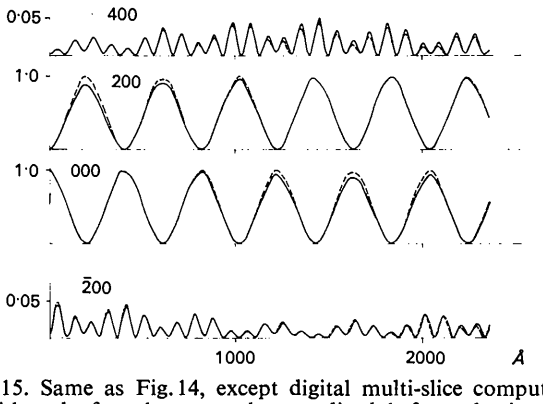


Fig. 15. Same as Fig. 14, except digital multi-slice computed with only four beams and normalized before plotting to allow for absorption due to the neglected weak beams.

† The digital calculation using the multi-slice method of Goodman & Moodie (1968) implementing equation (2) can be considered accurate to within the limits of error required, since the technique is well proven by agreement with experiment (Goodman & Lehmpfuhl, 1967) and various checks on computational accuracy are readily performed at all stages of the calculation (Goodman & Moodie, 1968).

in the normal way by the settings of the $\zeta$ potentiometers and the multipliers are used to give a point to point scan across the convergent beam discs. Apart from the multipliers very little additional hardware is required since for small angles the change in angle $\Delta\theta$ across a disc is linearly related to the change in each $\zeta_n$ by the relation $\Delta\zeta_n=(2\theta_n/\lambda)\Delta\theta$, where $\theta_n$ is the Bragg angle.

The intensities from distorted crystals are given by solving equation (45) of Howie & Whelan (1961) rewritten in the present notation as

$$\frac{dU_n}{dz}=2\pi i(\zeta_n+\beta'_n)U_n+i\sigma\sum_h E_{n-h}\,.\,U_h\,, \qquad (8)$$

where $\beta'_n=d[\mathbf{g}\,.\,\mathbf{R}(z)]/dz$ and $\mathbf{g}$ is the reciprocal lattice vector and $\mathbf{R}(z)$ the vector describing the displacement of the lattice at a depth $z$. Two function generators giving the $x$ and $y$ components of $d\mathbf{R}/dz$ are sufficient to permit the calculation of $\beta'_n$ for all $n$, since

$$\beta'_n=|\mathbf{g}_n|\,.\left(c_n\frac{dR_x}{dz}+d_n\frac{dR_y}{dz}\right),$$

where $c_n$ and $d_n$ are constants defining the angle between $\mathbf{g}$ and $\mathbf{R}$. Changing the slope of a ramp function generator which feeds the function generators allows the depth of the distortion within the crystal to be varied with the twist of a knob.

The $n$-beam electron microscope image of dislocations within a crystal can be rapidly obtained by using the foregoing technique on analog computers equipped with independently switched integrators and control logic.

In conclusion, the analog computer is seen as an invaluable adjunct to the digital machine in the field of dynamic electron diffraction computation when it is sufficient to include the interactions between a few strong beams. Additionally the analog circuit offers a fresh way of visualizing diffraction problems.

It is a pleasure to acknowledge the stimulating and helpful discussion of P. Goodman and A. F. Moodie and their continued interest in the work. The author is indebted to A. F. Moodie for acquainting him with the arguments in §2.

### References

BRILLOUIN, L. (1946). *Wave Propagation in Periodic Structures*. New York: McGraw-Hill.
COWLEY, J. M. & MOODIE, A. F. (1957). *Acta Cryst.* **10**, 609.
COWLEY, J. M. & MOODIE, A. F. (1962). *J. Phys. Soc. Japan*, **17**, Supp. BII, 86.
FUJIWARA, K. (1961). *J. Phys. Soc. Japan*, **16**, 2226.
GOODMAN, P. & LEHMPFUHL, G. (1967). *Acta Cryst.* **22**, 14.
GOODMAN, P. & MOODIE, A. F. (1968). To be published.
HEIDENREICH, R. D. (1950). *Phys. Rev.* **77**, 271.
HOWIE, A. (1963). *Proc. Roy. Soc.* A**271**, 268.
HOWIE, A. & WHELAN, M. J. (1961). *Proc. Roy. Soc.* A**263**, 217.
KAMBE, K. (1954). *Acta Cryst.* **7**, 777.
KAMBE, K. (1957). *J. Phys. Soc. Japan*, **12**, 13, 25.
KORN, G. A. & KORN, T. M. (1964). *Electronic Analog and Hybrid Computers*. New York: McGraw-Hill.
MOODIE, A. F. (1965). *Proc. Intern. Conf. Electron Diffraction and Crystal Defects*, Melbourne, ID–1.
TAKAGI, S. (1962). *Acta Cryst.* **15**, 1311.
TOURNARIE, M. (1961). *J. Phys. Soc. Japan*, **17**, Supp. BII, 98.

*Acta Cryst.* (1968). A**24**, 543

# Indexing of X-Ray Powder Patterns. Part I. The Theory of the Triclinic Case

BY V. VAND* AND G. G. JOHNSON, JR.

*Materials Research Laboratory and Department of Geochemistry and Mineralogy, The Pennsylvania State University, University Park, Pennsylvania* 16802, *U.S.A.*

(*Received* 24 *February* 1967 *and in revised form* 18 *May* 1967)

In a triclinic system, the squares of reciprocal spacings of any seven linearly independent X-ray powder lines which belong to the same lattice fulfill a Diophantine equation containing their Miller indices, which involves a $7\times7$ determinant. This can be expanded in minors which are integers. Theory is developed which breaks the problem of solving this equation into smaller steps, more easily amenable to numerical evaluation. The triclinic case has not yet been tried on a practical example, but the method has been already used in practice for systems of higher symmetry, for which the computational labor is much reduced.

## Introduction

It would appear from literature that the indexing problem for a triclinic system is very unlikely to succeed in practice. Most authors restrict themselves to special cases: no arbitrary angles in the unit cell (Hesse, 1948; Lipson, 1949; Stosick, 1949), or with unusual classes of compounds, such as long-spacing compounds (Vand, 1948). The method of Ito (Runge, 1917; Ito, 1950) attacks the problem from the low symmetry

* Deceased 4 April 1968.